Salicylideneaniline-Based Covalent Organic Frameworks

Quertinmont, Jean; Maschio, Lorenzo; Datta, Ayan; Champagne, Benoît

Published in:
Journal of Physical Chemistry C: Nanomaterials and interfaces

DOI:
10.1021/acs.jpcc.0c07672

Publication date:
2020

Document Version
Publisher's PDF, also known as Version of record

THE JOURNAL OF PHYSICAL CHEMISTRY C

pubs.acs.org/JPCC Article

Salicylideneaniline-Based Covalent Organic Frameworks: A New Family of Multistate Second-Order Nonlinear Optical Switches

Jean Quertinmont, Lorenzo Maschio, Ayan Datta, and Benoît Champagne*

Cite This: J. Phys. Chem. C 2020, 124, 24451−24459 Read Online

ACCESS | Metrics & More | Article Recommendations | Supporting Information

ABSTRACT: This work demonstrates that covalent organic frameworks (COFs) can exhibit large second-order nonlinear (NLO) responses and that these NLO responses can be modulated as a function of successive enol-imine/keto-enamine tautomerisms, leading to efficient solid-state second-order NLO switches. The proof of concept is given by evidencing, by means of periodic boundary condition (time-dependent) density functional theory calculations, the large amplitudes of the second-order NLO susceptibility, $\chi^{(2)}$, of two-dimensional COFs built from the assembly of tris(*N*-salicylideneaniline) units as well as their variations when switching between keto and enol forms. Calculations further demonstrate the key role of symmetry, that is, the distribution of enol and keto functions in the unit cell, on the $\chi^{(2)}$ values as well as on their dipolar/octupolar character.

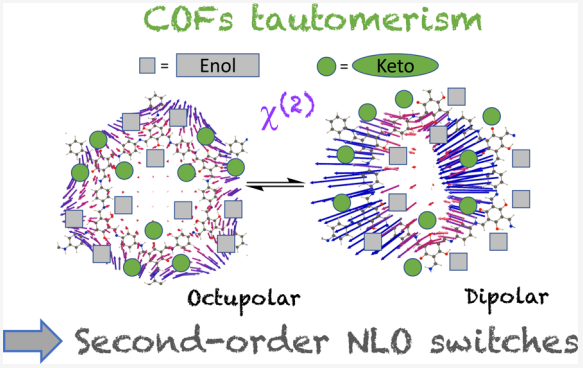

INTRODUCTION

Covalent organic frameworks (COFs) are porous crystalline materials built from strong covalent bonds between light elements.[1] The high accessible surface area and the mechanical robustness of these crystalline polymer networks make them ideal candidates as gas storage media, catalytic supports, sensing platforms, and energy storage devices, to cite a few applications.[2−4] These structural, electronic, thermodynamic, and kinetic properties can further be combined with linear and nonlinear optical (NLO) properties to elaborate multifunctional materials, in particular when the COFs switch between several forms. Very little is known about the NLO properties of COFs, whereas several studies have tackled those of the closely related metal organic frameworks (MOFs).[5] Among the few works on the NLO responses of COFs, in two recent papers, Biswal and co-workers[6,7] have reported the large nonlinear absorption (NLA) coefficient of regioregular porphyrin COFs. Moreover, by taking advantage of their precise spatial orientation in COFs, Deng and co-workers have revealed the two-photon absorption (TPA) potential of chromophores, which exhibits up to a 110-fold enhancement of their TPA cross section with respect to their molecular responses.[8] There is a continuing interest for materials exhibiting NLO responses because they are active components in applications such as laser modulation, data storage and processing, bioimaging, and optical transmission technologies,[9,10] and more studies are yet to be done to assess the potential of COFs. Note that both NLA and TPA are third-order NLO phenomena, whereas to the best of our knowledge, the second-order NLO responses of COFs (like the second harmonic generation, SHG) have not yet been studied. Among these NLO materials, when triggered by an external stimulus (change of pH or redox potential, irradiation by light, and complexation of an analyte), some present the ability to switch between two or several forms that display differences in their second- or third-order NLO responses. These systems are known as NLO switches,[11−14] and many examples have been reported, from molecules in solutions to functionalized surfaces and molecular crystals.[15−28] Still, in the crystal state, owing to compactness and the associated steric hindrance to structural switching, fewer NLO switches are known.[18,19] On the other hand, owing to the cavities in their structures, which can facilitate the motions of molecular fragments, COFs—as well as MOFs—are ideal candidates to exhibit NLO switching behavior.

As a matter of fact, the present contribution aims at assessing second-order NLO responses of a family of COFs built from the assembly of tris(*N*-salicylideneaniline) units by means of quantum chemical calculations and also their linear optical responses. The targeted linear responses are the linear optical (at pulsation ω) susceptibility, $\chi^{(1)}(-\omega;\omega) = \chi^{(1)}$, as well as the refractive indices and birefringence while the second-order NLO responses are the second-order NLO susceptibility associated with the SHG phenomenon, $\chi^{(2)}(-2\omega;\omega,\omega) = \chi^{(2)}$. As the first purpose, this paper gives the proof of concept that

Received: August 22, 2020
Revised: October 6, 2020
Published: October 22, 2020

Scheme 1. Structure of One Slab of COFs 1−5 in Their Fully Enol (Top) and Fully Keto (Bottom) Forms; in the Top Figure, the Hexagon Containing Six (Enol) Functions Is Represented

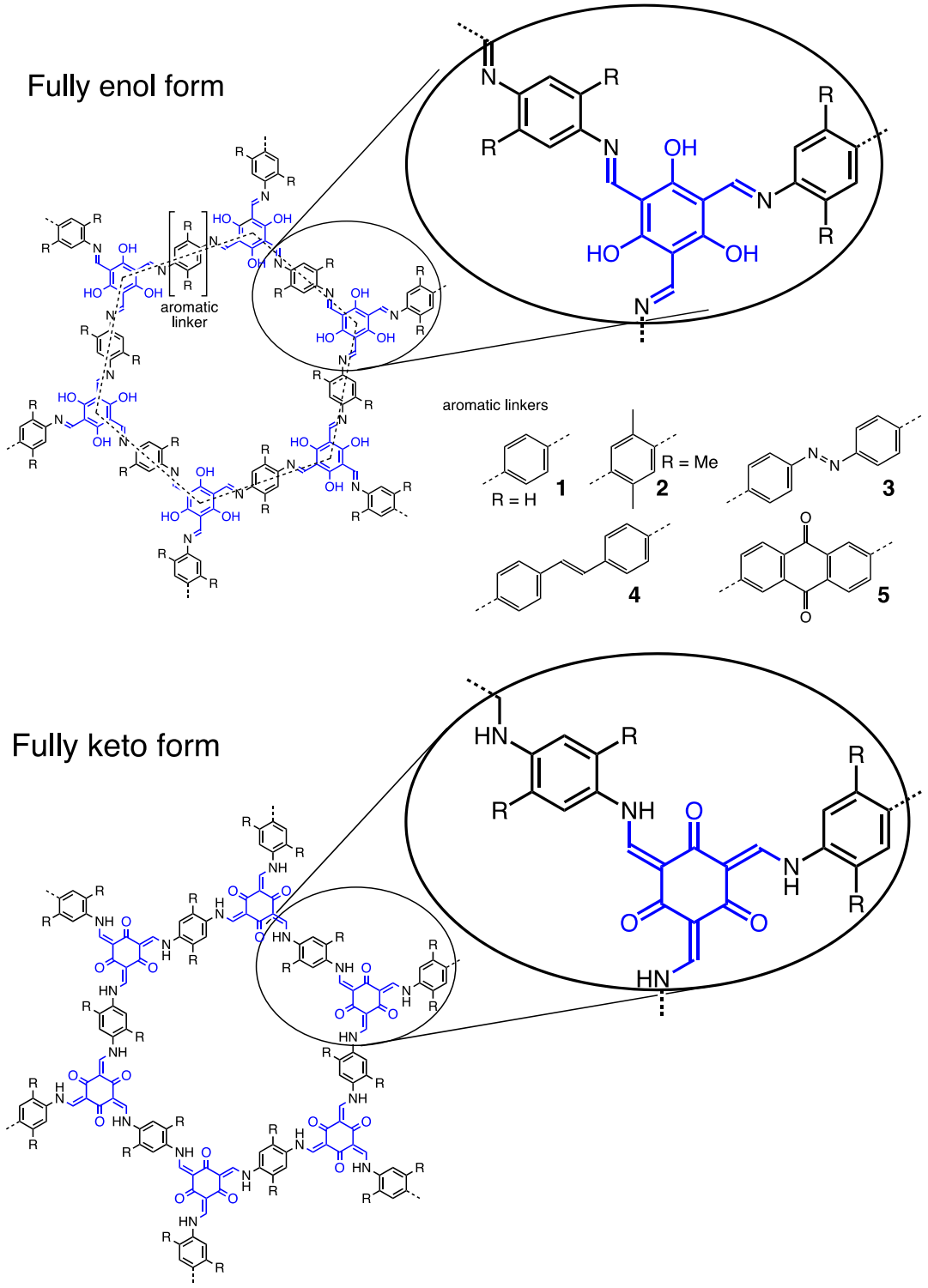

COFs can exhibit second-order NLO switching properties. On the basis of their recent experimental investigations[29−31] as well as of studies on the second-order NLO switching behavior of *N*-salicylideneaniline derivatives,[32] five crystalline two-dimensional (2D) COFs featuring enol-imine/keto-enamine tautomerism have been selected (Scheme 1). COFs **1** to **4** have been synthesized by Banerjee and co-workers[29,31] using Schiff base reaction of 1,3,5-triformylphloruglucinol with *p*-phenylenediamine (**1**), 2,5-dimethyl-*p*-phenylenediamine (**2**), 4,4′-azodianiline (**3**), and 4,4′-diaminostilbene (**4**), respectively. COFs **1** and **2** only differ by the presence of two methyl groups on the phenyl linker, while COFs **3** and **4** possess more extended linkers, namely, azobenzene and stilbene, respectively. Finally, COF **5** presents an anthraquinone linker and was originally designed for its charge storage ability.[30] From the viewpoint of modulating the second-order NLO responses,

https://dx.doi.org/10.1021/acs.jpcc.0c07672
J. Phys. Chem. C 2020, 124, 24451−24459

taking COF **1** as a reference, the donor character of the linker increases in the case of **2** and more substantially in the case of **3** and **4** with their azobenzene and stilbene donors, while the anthraquinone linker of COF **5** is an acceptor unit.

These COFs structures can be viewed as 2D networks of hexagons (Scheme 1), which are packed in an eclipsed pattern. Each of these hexagons defines a cavity, the size of which depends on the nature of the π-conjugated linker between the tris(*N*-salicylideneaniline) units, which are the nodes of the network (vertices of the hexagons). The inner part of each hexagon presents a total of six keto or enol functions. They are numbered according to Scheme S1. For each COF, this leads to a total of 14 tautomers (Table S1). Still, in this investigation, only periodic structures are considered in the sense that all the hexagons are identical. This prevents from studying highly disordered systems, but varying the enol and keto content of the unit cell already ensures chemical diversity. The corresponding structure representations are sketched in Table S1, together with the COF space groups.

Besides the proof-of-concept of COFs as second-order NLO switches, this paper addresses the following questions: (i) how large is the second-order NLO responses of *N*-salicylideneaniline-based COFs in comparison to reference molecular crystals? (ii) What is the amplitude of the variations of $\chi^{(2)}$ upon keto-to-enol switching? (iii) How to rationalize these linear and nonlinear responses in view of optimizing them?

METHODS

All computations were carried out using periodic boundary condition (PBC) density functional theory (DFT) as implemented in the CRYSTAL17 package.[33−35] The range-separated ωB97X[36] exchange−correlation (XC) functional was used with Pople's 6-31G(d,p) basis set (taken from Basis Set Exchange[37]). Starting from the single crystal X-ray diffraction structures, full geometry optimizations were performed. In recent contributions, some of us demonstrated the performance of the ωB97X XC functional to get geometries of molecular crystals in good agreement with single-crystal X-ray diffraction geometries, even without adding corrections for London dispersion interactions.[38,39] In addition, in ref 38, the ωB97X XC functional was shown to be suitable to predict whether the E or K form of *N*-salicylideneanilines is the most stable. Then, the electronic contribution to the linear [$\chi^{(1)}$] and second-order nonlinear [$\chi^{(2)}$] optical properties was enacted at the DFT level using the linear and quadratic response function methods implemented in a local version of CRYSTAL17.[40−44] This scheme (i) is based on the substitution of the unbound electric dipole moment operator ($\vec{r}$) by another perturbation operator ($\vec{\Omega}_{\vec{k}} = \vec{r} + \imath\vec{\nabla}_{\vec{k}}$), that is, the block diagonal in the same reciprocal $\vec{k}$-space as the unperturbed Fock matrix, (ii) takes advantage of the $2n + 1$ rule, and (iii) enables calculating both the static and dynamic responses. This approach presents some advantages to calculate the $\chi^{(1)}$ and $\chi^{(2)}$ responses because it provides these responses in a single step. In this way, contrary to other methods that have been employed to calculate the optical responses of molecular crystals and MOFs, this method does not suffer from various limitations: (i) in the cluster approach, the optical responses depend on the cluster size and shape as well as on the way the dangling bonds are saturated,[45] (ii) it does not involve a two-step procedure where molecular responses need to be computed first before evaluating the macroscopic ones,[46,47] and (iii) with respect to other PBC-based perturbative approaches, it does not require the use of a scissor operator to correct the underestimated band gaps.[48,49]

The number of nonequivalent nonzero $\chi^{(1)}$ and components depends on the space group (in particular, in centrosymmetric crystals, all $\chi^{(2)}$ tensor components vanish). These components are listed in Table S1. In addition to the tensor components, which are listed in the Supporting Information (besides the negligible $\chi^{(2)}_{XZZ}$ and $\chi^{(2)}_{YZZ}$), we have provided three invariants, their dipolar $|\chi^{(2)}_{J=1}|$ and octupolar $|\chi^{(2)}_{J=3}|$ components as well as their ratio, and the nonlinear anisotropy, $\rho = |\chi^{(2)}_{J=3}|/|\chi^{(2)}_{J=1}|$. These quantities, of which the full expressions can be found in ref 50 are generally considered for molecules and clusters but can also be generalized to COFs.[51,52] To visualize the $\chi^{(2)}$ tensor, the unit sphere representation (USR), initially proposed for the first hyperpolarizability tensor,[53] was adopted. It consists (i) in computing induced polarization,

$$\vec{P}_{\text{ind}} = \overleftrightarrow{\chi}^{(2)} : \vec{E}^2(\theta, \phi)$$

where the tensor nature of $\chi^{(2)}$ has been evidenced and $\vec{E}(\theta,\phi)$ is a unit vector of the electric field, of which the polarization direction is defined in spherical coordinates by the θ and ϕ angles, and (ii) by representing all the induced polarization vectors on a sphere centered on the center of mass of the primitive unit cell. This enables highlighting the directions where the second-order polarization is the strongest (it corresponds to the largest induced dipoles) and its orientation (the acceptor−donor direction), subsequently showing how much the $\chi^{(2)}$ response is dipolar/octupolar. These USRs were plotted using the DrawMol package.[54]

The excitation energies to the lowest dipole-allowed excited states were evaluated from the frequency dispersion of the dynamic $\chi^{(1)}(-\omega;\omega)$ response, with $\hbar\omega$ the incident photon energy. Indeed, time-dependent perturbation theory $\chi^{(1)}(-\omega;\omega)$ can be written under the form of a summation over the excited states and close to resonance where the contribution of each excited state (e) to frequency dispersion reads

$$\frac{\chi^{(1)}(-\omega;\,\omega)}{\chi^{(1)}(-0;\,0)} = \mathcal{F}(\omega) = \mathcal{R}(\omega) + \mathcal{I}(\omega)\imath$$
$$= \frac{\omega_{\text{eg}}{}^4 - \omega_{\text{eg}}{}^2\omega^2}{(\omega_{\text{eg}}{}^2 - \omega^2)^2 + \omega^2\Gamma_{\text{eg}}{}^2} + \frac{\omega_{\text{eg}}{}^2\omega\Gamma_{\text{eg}}}{(\omega_{\text{eg}}{}^2 - \omega^2)^2 + \omega^2\Gamma_{\text{eg}}{}^2}\imath$$

with $\mathcal{R}(\omega)$ and $\mathcal{I}(\omega)$ their real and imaginary parts, respectively. $\hbar\omega_{\text{eg}}$ is the corresponding excitation energy, and Γ_{eg} is the damping factor. So, at resonance, that is when $\hbar\omega$ matches a vertical excitation energy, the real part amounts to zero while its imaginary counterpart attains a maximum. The dynamic $\chi^{(1)}(-\omega;\omega)$ responses were calculated for a range of incident photon energies with $\Gamma_{\text{eg}} = \Gamma = 10^{-3}$ a.u. Using the above $\mathcal{F}(\omega)$ form for each transition, we evaluated by least-squares regression the $\hbar\omega_{\text{eg}}$ that gives the best fit to the calculated data. Both the real and imaginary components of the $\chi^{(1)}$ response were employed, and they gave very similar excitation energies. Illustrative results are given in Figures S1 and S2 to show the frequency dispersions, the fitting curves, and the corresponding excitation energies of COF **1** (4K2E/1-

https://dx.doi.org/10.1021/acs.jpcc.0c07672
J. Phys. Chem. C 2020, 124, 24451−24459

2 and 5K1E). For these packed-slabs materials, the in-plane diagonal components of the $\chi^{(1)}$ response present resonances between 2 and 4 eV, demonstrating that for these low-energy excitations, the dipole transition moments are in-plane polarized. On the other hand, optical transitions polarized along Z, that is, perpendicular to the COF slabs, are associated with $\chi_{ZZ}^{(1)}$, appear above 6 eV, and are not discussed in this work.

To enact CRYSTAL17 calculations, default convergence criteria were used while the irreducible Brillouin zone was sampled on a 4 4 6 grid (SHRINK keyword). The truncation criteria for the Coulomb and exchange integrals were set to 7 7 7 7 16 (TOLINTEG keyword) for the geometry optimization calculations while for the calculation of the linear and NLO properties, TOLINTEG was set to tighter criteria: 10 10 10 30 100.

RESULTS AND DISCUSSION

Geometries and Relative Stability. Full geometry optimizations were carried out at the ωB97X/6-31G(d,p) level for the eclipsed structures, starting from the structures taken from refs.[29,31] This choice is substantiated by the analysis of the powder X-ray diffraction data, which led to conclude that these COFs adopt an eclipsed rather than a staggered structure.[29−31] The relative energies demonstrate that the fully keto form is the most stable and that the first keto-to-enol transformation costs between 32 and 36 kJ/mol (Table 1).

Table 1. Relative Energies (kJ/mol per Primitive Cell) of the Different Tautomers of COFs 1−5 as Evaluated at the PBC/ωB97X/6-31G(d,p) Level of Approximation[a]

tautomer		1	2	3	4	5
6K0E		0.0	0.0	0.0	0.0	0.0
5K1E		32.5	33.4	36.0	34.9	36.0
4K2E	1−2	63.6	65.6	71.2	69.2	71.4
	1−3	57.2	59.0	64.3	62.0	64.8
	1−4	68.4	69.4	72.8	70.8	73.0
3K3E	1−2−3	86.6	89.7	98.4	95.5	99.1
	1−3−4	92.5	94.5	100.8	97.7	101.6
	1−3−5	61.5	67.9	71.4	68.1	72.6
	1−4−5	92.0	94.4	100.6	97.5	101.4
2K4E	1−2−3−4	114.0	117.5	127.3	123.2	128.2
	1−2−4−5	120.5	123.0	130.1	125.7	131.3
	1−3−4−5	95.2	101.6	107.2	103.0	108.2
1K5E		121.6	128.0	135.4	130.0	136.9
0K6E		127.6	135.7	142.5	136.0	144.3

[a]The relative energies are evaluated with respect to the most stable tautomer of each COF.

Then, for the second keto-to-enol transformation, the energy cost depends on the pair of keto sites. If the transformation occurs on a different tris(*N*-salicylideneaniline) node, the same amount of energy (sites 1 and 2) or a bit more (sites 1 and 4) is required. On the other hand, if it occurs on the same node, the needed energy is smaller (25−28 kJ/mol). The third transformation is again less demanding if it occurs on the same node (sites 1, 3, and 5) with energy between 4 and 9 kJ/mol. This lower energy cost results from the fact that the combination of three enol functions on the same node restores the aromaticity of the ring (see also below for the discussion on the geometry). Finally, the energy cost to go from 6K0E to 0K6E is about twice larger than to switch between 6K0E and 3K3E/1−3−5, demonstrating a good extent of the additive character and the weak impact of the adjacent nodes.

The aromaticity driving force was substantiated here by geometrical criteria, the CC bond lengths, and the bond length alternation (BLA) in the ring. So, considering the node with the sites 1, 3, and 5, the average CC bond length in the ring ranges from 1.465 Å in 6K0E to 1.449 Å in 5K1E, 1.431 Å in 4K2E/1−3, and 1.414 Å in 3K3E/1−3−5 for COF **1** (similar results are obtained for the other set of rings, but the nomenclature is different). Then, BLA was evaluated as the average bond length differences between adjacent CC bonds of the ring of the same node. Considering 6K0E, 5K1E, 4K2E/1−3, and 3K3E/1−3−5, the ring BLA of **1** amounts to 0.010, 0.018, 0.018, and 0.003 Å, respectively. As expected, 3K3E/1−3−5 is the most aromatic with a negligible BLA and then comes 6K0E, where there are three keto functions on each ring (BLA = 0.010 Å). Finally, 5K1E and 4K2E/1−3 combine one enol and two keto functions or vice versa, which increases the BLA by a factor of two with respect to 6K0E. Looking at the bond lengths of the molecular segments that are mostly affected by the keto-to-enol switching (O═C−C═C−NH → HO−C═C−C═N), the variations as determined at the same PBC/ωB97X/6-31G(d,p) level are typically 0.01−0.02 Å larger in the present tris(*N*-salicylideneaniline) units than in more simple *N*-salicylideneaniline, like (*E*)-2-methoxy-6-(pyridine-3-yliminomethyl)phenol (PYV3), highlighting cooperative effects in the former ones.[38] Similar geometrical effects are observed for the four other COFs as well.

Mulliken charge distributions have been analyzed to highlight which subunits are electron donors or acceptors. For all COFs and no matter what is the K/E ratio, the aromatic linkers (Scheme 1) are donors, with charges between 1.2 e and 1.6 e. The charges on the two tris(*N*-salicylideneaniline) nodes, the electron acceptors, are very similar, with amplitudes generally smaller by 0.1 e. This demonstrates a small or negligible charge transfer between them, and therefore, the second-order NLO responses are not expected to have a charge-transfer origin like in push−pull π-conjugated systems. These results were confirmed by additional Hirshfeld charge calculations. When the K/E ratio decreases, the charge transfer decreases by up to 0.20−0.25 e. Finally, the amount of charge transfer increases from COF **5** (1.40/1.19 e) to **3** (1.50/1.28 e), to **4** (1.53/1.33 e), to **1** (1.55/1.31 e), and to **2** (1.62/1.37 e), where the first value corresponds to the charge on the aromatic linker for the all-keto form while the second for the all-enol form. Again, as analyzed subsequently, there is no evident correlation between these charge transfer amplitudes and the $\chi^{(2)}$ responses of the different tautomers.

Excitation Energies. Using the optimized structures, the two lowest-energy dipole-allowed excitation energies ($\hbar\omega_{eg}$) and band gaps ($\Delta E_{HL} = \varepsilon_{LUCO} - \varepsilon_{HOCO}$, with the LUCO and HOCO (the lowest-unoccupied crystalline orbital and the highest-occupied crystalline orbital), were evaluated. The excitation energies were calculated by least-squares fitting the few-state approximation $\chi^{(1)}(-\omega;\omega)$ expression to a set of complex $\chi^{(1)}(-\omega;\omega)$ values calculated for incident photon energies between 0.06 and 0.22 a.u. and with a damping factor of 10^{-3} a.u (Figures S1 and S2). These electronic transitions are polarized in the plane (XY) of the COF slabs. For COF **1**, they present a complex dependence on the tautomer form (Table 2).

For hexagonal symmetry (6K0E, 3K3E/1−3−5, and 0K6E), these transitions are degenerate and respectively polarized

https://dx.doi.org/10.1021/acs.jpcc.0c07672
J. Phys. Chem. C 2020, 124, 24451−24459

Table 2. Band Gap and Excitation Energies (eV) of the Tautomers of COF 1 as Evaluated at the PBC/ωB97X/6-31G(d,p) Level of Approximation[a]

tautomer		band gap	1st excitation energy	2nd excitation energy
6K0E		5.85	3.40[b]	
5K1E		5.68 (−0.17)	3.28 (−0.12)	3.43 (0.03)
4K2E	1−2	5.65 (−0.20)	3.23 (−0.17)[c]	3.41 (+0.01)[d]
	1−3	5.63 (−0.22)	3.27 (−0.13)[c]	3.41 (+0.01)[d]
	1−4	5.50 (−0.35)	3.15 (−0.25)	3.49 (0.09)
3K3E	1−2−3	5.67 (−0.18)	3.18 (−0.22)	3.40 (0.00)
	1−3−4	5.47 (−0.38)	3.24 (−0.16)	3.34 (−0.06)
	1−3−5	6.02 (0.17)	3.44 (0.04)[b]	
	1−4−5	5.50 (−0.35)	3.18 (−0.22)	3.43 (0.03)
2K4E	1−2−3−4	5.58 (−0.27)	3.17 (−0.23)	3.32 (−0.08)
	1−2−4−5	5.32 (−0.52)	3.15 (−0.25)[c]	3.43 (0.03)[d]
	1−3−4−5	5.82 (−0.03)	3.31 (−0.09)	3.49 (0.09)
1K5E		5.72 (−0.13)	3.30 (−0.10)	3.45 (0.05)
0K6E		6.27 (0.42)	3.53 (0.13)[b]	

[a]In parentheses are given the differences with respect to the 6K0E tautomer. [b]This transition is degenerate. One is polarized along *X* while the other along *Y*. [c]This transition is polarized along *X*. [d]This transition is polarized along *Y*. Otherwise, the transitions are polarized in the *XY* plane.

along the *X* and *Y* axis. For the other space symmetries, the energy splitting ranges from 0.15 to 0.35 eV. The first excitation energy of the all-keto form (3.40 eV) is slightly smaller than for its corresponding all-enol form (3.53 eV), while mixing enol and keto tautomers results generally in smaller first excitation energies (the smallest value is achieved for 4K2E/1−4 and 2K4E/1−2−4−5 with a value of 3.15 eV). The exception is 3K3E/1−3−5 where one center bears only enol forms (1, 3, and 5 sites, Scheme S1), while the other bears only keto forms (2, 4, and 6 sites, Scheme S1). In that case, the degenerate first excitation energies are slightly larger than those in 6K0E (but slightly smaller than in 0K6E) and also larger than those for the other 3K3E tautomers. This is attributed to aromaticity, which opens the gap slightly. A similar effect is observed in the case of 2K4E/1−3−4−5, for the same reason. To a good extent, the variations of $\hbar\omega_{eg}$ follow those of the band gap, though the latter is systematically larger by about 2 eV. The variations of the second excitation energy are smaller. Considering both the first and second excitation energies, the rather small E-to-K shift (less than 0.4 eV) contrasts with the large enol-to-keto bathochromic shift observed for simple salicylideneanilines[55] as well as for tris(salicylideneaniline)[56] derivatives in solution. Therefore, the variations of the linear and NLO susceptibilities are not expected to be driven by changes in the excitation energies.

The lowest excitation energies were then evaluated for the full-keto and full-enol tautomers of the other COFs (Figure 1) highlighting (i) the systematic smaller values by 0.08−0.15 eV of the full keto form, (ii) the relatively minor modifications when increasing the size of the π-conjugated linker, and (iii) the largest values obtained in the case of an anthraquinone linker.

Refractive Indices and Birefringence. Consistently with the small variations of the optical gap and excitation energies as a function of tautomer, for a given COF, the refractive indices and birefringence also depend hardly on the E/K distribution (Table S2). On the other hand, the variations are much larger among the different COFs, which can be explained by their different porosity (empty space) as a function of the size of the linker (Table 3). This is evidenced by the differences between

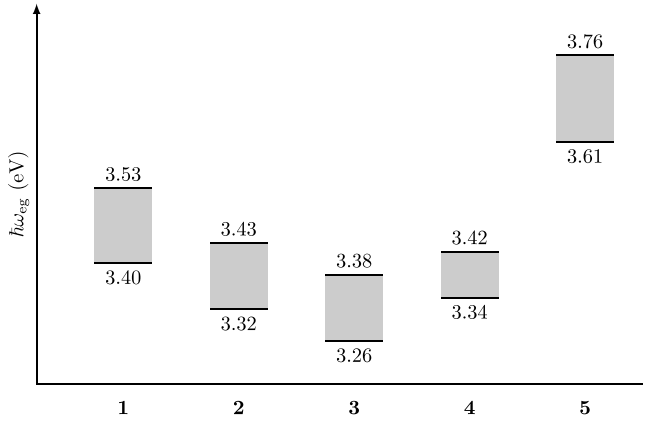

Figure 1. Excitation energies ($\hbar\omega_{eg}$, eV) of the 6K0E (bottom) and 0K6E (top) tautomers of COFs **1**−**5**.

Table 3. Linear Optical Properties of the 6K0E (0K6E) Tautomers of the Different COFs: Average Refractive Index in the *XY* Plane, $n_{XY} = (n_X + n_Y)/2$, Refractive Index along *Z*, n_Z, and Birefringence, $\delta = (n_{XY} - n_Z)$[a]

COFs	n_{XY}	n_Z	δ
1	1.479 (1.481)	1.110 (1.114)	0.369 (0.367)
2	1.505 (1.508)	1.146 (1.150)	0.359 (0.358)
3	1.352 (1.347)	1.077 (1.079)	0.275 (0.269)
4	1.338 (1.338)	1.074 (1.076)	0.264 (0.262)
5	1.370 (1.367)	1.095 (1.097)	0.276 (0.270)

[a]All values were evaluated at the PBC/ωB97X/6-31G(d,p) level of approximation for $\omega = 0$.

the larger $n_{XY} = (n_X + n_Y)/2$ values of COFs **1** and **2** having smaller aromatic linkers—and therefore smaller cavities—and the smaller n_{XY} values of COFs **3** and **4** having larger cavities while COF **5** presents intermediate values. Similarly, the birefringence is larger for COFs **1** and **2** than for COFs **3**, **4**, and **5**.

Second-Order NLO Susceptibilities. With respect to the linear responses, the $\chi^{(2)}$ tensor components and invariants (Tables 4 and S3−S6) present stronger dependence on the tautomer, as expected for an odd-order property. COFs appear, therefore, as potential second-order solid-state NLO switches. When comparing to reference compounds like urea, the amplitude of the COFs $\chi^{(2)}$ tensor components is large but still smaller than in 2-methyl-4-nitroaniline (MNA). Indeed, for the former, $\chi^{(2)}_{XYZ}$ amounts to 2.4 pm/V at 1064 nm,[57] while for the latter, $\chi^{(2)}_{111}$ gets as large as 300 pm/V at the same wavelength.[58]

Results in Tables S3−S6 show that the largest component is usually $\chi^{(2)}_{XXX}$, then $\chi^{(2)}_{YYY}$, and finally the off-diagonal ones. For all COFs and all tautomer forms except 3K3E/1−3−5, the dipolar contribution is larger than the octupolar one and typically twice larger (Table 4). In the case of 3K3E/1−3−5, which presents a hexagonal structure, the response is fully octupolar. The difference between the dipolar and octupolar responses of the COF **1** is further evidenced by their USRs (Figure 2).

No matter which π-linker is considered, the largest responses are generally obtained for the 3K3E and 2K4E tautomer forms,

https://dx.doi.org/10.1021/acs.jpcc.0c07672
J. Phys. Chem. C 2020, 124, 24451−24459

Table 4. Dipolar and Octupolar Components to the Static $\chi^{(2)}$ (pm/V) and Their Ratio (ρ) for the Tautomers of COF 1−5 as Evaluated at the PBC/ωB97X/6-31G(d,p) Level of Approximation[a]

tautomer		1	2	3	4	5
		$\lvert\chi^{(2)}_{J=1}\rvert$, $\lvert\chi^{(2)}_{J=3}\rvert$, ($\rho = \lvert\chi^{(2)}_{J=3}\rvert/\lvert\chi^{(2)}_{J=1}\rvert$)				
5K1E		5.4, 2.7 (0.51)	5.6, 2.9 (0.51)	3.3, 1.7 (0.51)	2.9, 1.5 (0.50)	2.3, 1.4 (0.59)
4K2E	1−2	10.2, 5.2 (0.51)	10.7, 5.4 (0.51)	5.9, 3.0 (0.50)	5.3, 2.7 (0.50)	4.2, 2.1 (0.50)
	1−3	7.9, 4.0 (0.51)	8.1, 4.1 (0.51)	4.8, 2.4 (0.50)	4.4, 2.2 (0.50)	3.0, 2.0 (0.67)
3K3E	1−2−3	15.6, 7.9 (0.51)	15.9, 8.1 (0.51)	8.7, 4.4 (0.50)	7.9, 4.0 (0.50)	5.7, 3.0 (0.52)
	1−3−4	7.4, 3.8 (0.52)	7.7, 3.9 (0.51)	4.2, 2.1 (0.51)	3.8, 1.9 (0.50)	2.7, 1.6, (0.58)
	1−3−5[b]	0, 2.2 (∞)	0, 2.4 (∞)	0, 1.1 (∞)	0, 1.3 (∞)	0, 1.0 (∞)
	1−4−5	7.0, 3.6 (0.51)	7.1, 3.7, (0.52)	4.4, 2.2, 0.51	3.9, 2.0 (0.51)	2.8, 1.5 (0.54)
2K4E	1−2−3−4	15.8, 8.0 (0.51)	16.0, 8.1 (0.50)	8.8, 4.5, 0.50	8.1, 4.0 (0.50)	5.6, 2.8 (0.50)
	1−3−4−5	5.9, 4.0 (0.68)	6.1, 4.2 (0.68)	3.3, 2.1, 0.65	3.0, 2.0 (0.68)	2.4, 1.4 (0.59)
1K5E		8.4, 5.0 (0.59)	8.6, 5.0 (0.59)	4.8, 2.7, 0.58	4.4, 2.5 (0.57)	3.1, 1.8, 0.57

[a]Centrosymmetric tautomers (6K0E, 4K2E/1−4, 2K4E/1−2−4−5, and 0K6E) have zero values and these are not reported. [b]The anisotropy factors of the 3K3E/1−3−5 tautomers were set to infinity, though due to numerical precision, their $\lvert\chi^{(2)}_{J=1}\rvert$ values were not exactly zero.

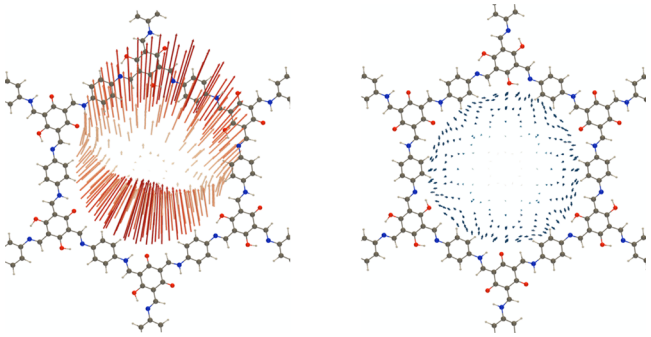

Figure 2. USR of the static $\chi^{(2)}$ tensor of COF **1** in its 3K3E/1−2−3 (left, dipolar character) and 3K3E/1−3−5 (right, octupolar character) as calculated at the PBC/ωB97X/6-31G(d,p) level of approximation (USR factor of 1.0).

followed by 4K2E, 1K5E, and 5K1E. Considering the successive switching of the keto functions into enol ones, $\chi^{(2)}_{XXX}$ takes the following values (in pm/V): 0 (6K0E), 3.5 (5K1E), 7.3 (4K2E/1−3, as the most stable form), 0.8 (3K3E), −2.8 (2K4E), 3.9 (1K5E), and 0 (0K6E). These values demonstrate that switching the keto functions has a clear impact on the second-order NLO responses. How large it will be in practice remains to be seen since the keto-to-enol transformation will most probably not occur in the same way in all the unit cells.

Comparing their largest $\chi^{(2)}$ tensor components ($\chi^{(2)}_{YYY}$), 1K5E and 5K1E demonstrates that the keto form has stronger potential than the enol form to achieve large $\chi^{(2)}$ responses. At first sight, this appears contradictory because in 1K5E, there are more enol than keto units. However, 1K5E differs with respect to the centrosymmetric 0K6E by only one keto function, and therefore, one can attribute the $\chi^{(2)}$ response to the unique keto site that breaks the centrosymmetry. As discussed above the keto forms are associated with slightly smaller band gaps and excitation energies but also with smaller unit cell polarization (cfr Mulliken charges). Large second-order NLO responses were also observed for the keto form of a 2-hydroxy-1-naphthaldehyde derivative,[59] but this is not a general conclusion since the keto/enol relative values depend strongly on the nature and position of the donor and acceptor groups on the aniline core.[60]

The $\chi^{(2)}$ response depends also on the nature of the π-linker, with a clear trend: **2** > **1** > **3** > **4** > **5**. To a good extent, these variations and ordering originate from the length of the π-linker: the longer the π-linker, the larger the primitive unit cell (PUC) volume (Table S7) and, therefore, for a given "molecular" β response, the macroscopic response gets smaller [$\chi^{(2)} = \beta/2\varepsilon_0 V_{PUC}$]. This explains the differences between COFs **1** and **2** on the one hand and COFs **3** and **4** on the other hand. The larger response of **2** with respect to **1** is attributed to the better donor character of its π-linker, bearing two methyl groups. When putting aside the effects of the volume, the largest value is achieved with COF **3** but it is diluted in the larger volume. The smallest responses are observed for COF **5**, owing to its π-linker with the smallest donor effect.

Figure 3 displays the typical frequency dispersion of $\chi^{(2)}$ of these COFs derivatives, which deviates from the linear

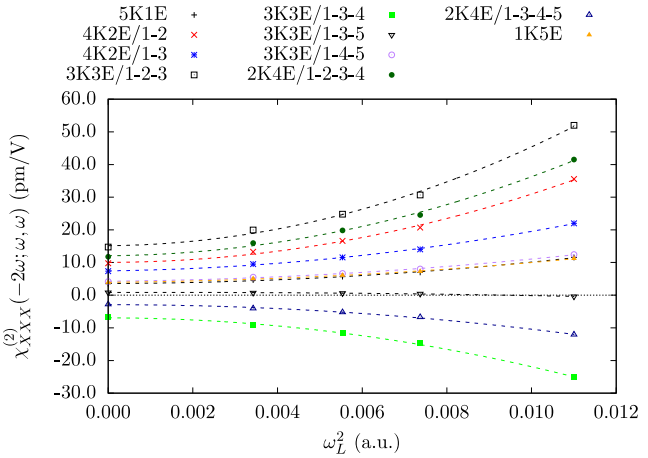

Figure 3. Frequency dispersion of the $\chi^{(2)}_{XXX}$ tensor component of COF **1** for its different non-centrosymmetric tautomer forms as calculated at the PBC/ωB97X/6-31G(d,p) level of approximation. The lines are the quadratic fits in $\omega_L^2 = 6\omega^2$.

dependence in ω_L^2, though the first electronic resonance is still far away. The last points in the graph correspond to a photon energy $\hbar\omega$ of 1.16 eV (λ = 1064 nm) that is a SHG energy of 2.32 eV, whereas the first resonance is at 3.3 eV or higher.

https://dx.doi.org/10.1021/acs.jpcc.0c07672
J. Phys. Chem. C 2020, 124, 24451−24459

CONCLUSIONS AND OUTLOOK

PBC DFT calculations have been performed to characterize the second-order NLO responses, $\chi^{(2)}$, of crystalline 2D COFs built from the assembly of tris(*N*-salicylideneaniline) units displaying tautomerisms between enol-imine and keto-enamine forms. At a typical laser wavelength of 1064 nm, the $\chi^{(2)}$ amplitudes are 1 order of magnitude larger than for the reference urea crystal but still about 1 order of magnitude smaller than in the crystal of MNA, a push−pull π-conjugated compound. These results are the first to demonstrate that COFs can exhibit large second-order nonlinear responses. The symmetry as well as the unit cell size have been found to be the key parameters in order to design COFs with improved $\chi^{(2)}$ responses. Indeed, larger π-linkers between the tris(*N*-salicylideneaniline) nodes of the COFs lead to a reduction of the $\chi^{(2)}$ responses, which can be interpreted as a kind of dilution since the porosity of the COFs increases. The symmetry was shown to have an impact on the $\chi^{(2)}$ amplitudes as well as on their dipolar *versus* octupolar character. Moreover, these calculations demonstrate that the NLO responses of these COFs can be modulated as a function of the successive enol-imine/keto-enamine tautomerisms, leading to efficient solid-state second-order NLO switches. On the other hand, for the investigated COFs, the linear optical responses (excitation energies, refractive indices, and birefringence) exhibit smaller variations as a function of the nature of the π-linker or as a function of keto−enol switching.

We hope that this computational solid-state chemistry proof-of-concept will stimulate experimental investigations on the measurement of the NLO responses of COFs on their variations as a function of successive switching operations between the enol-imine and keto-enamine forms as well as on the design of multifunctional materials, owing to their already-recognized catalytic and sensing properties. Along these lines, following a recent investigation demonstrating that merocyanine/spiropyran second-order NLO molecular switches can be used as efficient cation sensors because they can discriminate between their size and their charge,[61] it is also worth investigating how the K/E ratios and subsequently the NLO responses change when anchoring metal atoms on the keto-enamine/enol-imine functions. Moreover, modulating the π-linker by adding strong donor/acceptor units also deserves to be investigated since it turned out to be a rewarding strategy to optimize molecular NLO switches.[14]

ASSOCIATED CONTENT

Supporting Information

The Supporting Information is available free of charge at https://pubs.acs.org/doi/10.1021/acs.jpcc.0c07672.

Unit cells and numbering code of the tautomers in the Cartesian space; space groups of the different tautomers and the list of independent nonzero tensor components; frequency dispersions of $\chi^{(1)}$ and determination of the excitation energies; linear and second-order NLO properties; and PUC volumes (PDF)

AUTHOR INFORMATION

Corresponding Author

Benoît Champagne − *Theoretical Chemistry Laboratory, Unit of Theoretical and Structural Physical Chemistry, Namur Institute of Structured Matter, University of Namur, B-5000 Namur, Belgium;* orcid.org/0000-0003-3678-8875; Email: benoit.champagne@unamur.be

Authors

Jean Quertinmont − *Theoretical Chemistry Laboratory, Unit of Theoretical and Structural Physical Chemistry, Namur Institute of Structured Matter, University of Namur, B-5000 Namur, Belgium;* orcid.org/0000-0001-9408-1451

Lorenzo Maschio − *Dipartimento di Chimica, Università di Torino, 10125 Torino, Italy;* orcid.org/0000-0002-4657-9439

Ayan Datta − *School of Chemical Sciences, Indian Association for the Cultivation of Science, 700032 Kolkata, India;* orcid.org/0000-0001-6723-087X

Complete contact information is available at: https://pubs.acs.org/10.1021/acs.jpcc.0c07672

Notes

The authors declare no competing financial interest.

ACKNOWLEDGMENTS

J.Q. thanks the "Actions de Recherche Concertées" (ARC) de la Direction générale de l'Enseignement non obligatoire et de la Recherche scientifique—Direction de la Recherche scientifique—Communauté française de Belgique, under convention no. 15/20-068 for his PhD grant. J.Q., A.D., and B.C thank BELSPO for fundings through the Indo-Belgian Research and Technology Cooperation project BL/13/IN16 entitled "Optical Properties of MOFS/COFS". The authors thank N. Mandal for preliminary investigations on this topic. The calculations were performed on the computers of the Consortium des Équipements de Calcul Intensif (CÉCI, http://www.ceci-hpc.be) and particularly those of the Technological Platform of High-Performance Computing, for which the authors gratefully acknowledge the financial support of the FNRS-FRFC, of the Walloon Region, and of the University of Namur (Conventions no. 2.5020.11, GEQ U.G006.15, 1610468, and RW/GEQ2016), as well as of zenobe, the Tier-1 facility of the Walloon Region (Convention 1117545).

REFERENCES

(1) Diercks, C. S.; Yaghi, O. M. The Atom, the Molecule, and the Covalent Organic Framework. *Science* **2017**, *355*, No. eeal1585.

(2) Waller, P. J.; Gándara, F.; Yaghi, O. M. Chemistry of Covalent Organic Frameworks. *Acc. Chem. Res.* **2015**, *48*, 3053−3063.

(3) Kandambeth, S.; Dey, K.; Banerjee, R. Covalent Organic Frameworks: Chemistry beyond the Structure. *J. Am. Chem. Soc.* **2019**, *141*, 1807−1822.

(4) Geng, K.; He, T.; Liu, R.; Dalapati, S.; Tan, K. T.; Li, Z.; Tao, S.; Gong, Y.; Jiang, Q.; Jiang, D. Covalent Organic Frameworks: Design, Synthesis, and Functions. *Chem. Rev.* **2020**, *120*, 8814−8933.

(5) Wang, C.; Zhang, T.; Lin, W. Rational Synthesis of Noncentrosymmetric Metal-Organic Frameworks for Second-Order Nonlinear Optics. *Chem. Rev.* **2012**, *112*, 1084−1104.

(6) Biswal, B. P.; Valligatla, S.; Wang, M.; Banerjee, T.; Saad, N. A.; Mariserla, B. M. K.; Chandrasekhar, N.; Becker, D.; Addicoat, M.; Senkovska, I.; Berger, R.; Rao, D. N.; Kaskel, S.; Feng, X. Nonlinear Optical Switching in Regioregular Porphyrin Covalent Organic Frameworks. *Angew. Chem., Int. Ed.* **2019**, *58*, 6896−6900.

(7) Samal, M.; Valligatla, S.; Saad, N. A.; Rao, M. V.; Rao, D. N.; Sahu, R.; Biswal, B. P. A Thiazolo[5,4-*d*]Thiazole-Bridged Porphyrin Organic Framework as a Promising Nonlinear Optical Material. *Chem. Commun.* **2019**, *55*, 11025−11028.

(8) Zhang, L.; Zhou, Y.; Jia, M.; He, Y.; Hu, W.; Liu, Q.; Li, J.; Xu, X.; Wang, C.; Carlsson, A.; Lazar, S.; Meingast, A.; Ma, Y.; Xu, J.; Wen, W.; Liu, Z.; Cheng, J.; Deng, H. Covalent Organic Framework for Efficient Two-Photon Absorption. *Matter* **2020**, *2*, 1049−1063.
(9) Verbiest, T.; Clays, K.; Rodriguez, V. *Second-Order Nonlinear Optical Characterizations Techniques: an Introduction*; CRC Press: New York, 2009.
(10) Reeve, J. E.; Anderson, H. L.; Clays, K. Dyes for Biological Second Harmonic Generation Imaging. *Phys. Chem. Chem. Phys.* **2010**, *12*, 13484−13498.
(11) Coe, B. J. Molecular Materials Possessing Switchable Quadratic Nonlinear Optical Properties. *Chem.—Eur. J.* **1999**, *5*, 2464−2471.
(12) Delaire, J. A.; Nakatani, K. Linear and Nonlinear Optical Properties of Photochromic Molecules and Materials. *Chem. Rev.* **2000**, *100*, 1817−1846.
(13) Asselberghs, I.; Clays, K.; Persoons, A.; Ward, M. D.; McCleverty, J. Switching of Molecular Second-Order Polarizability in Solution. *J. Mater. Chem.* **2004**, *14*, 2831−2839.
(14) Castet, F.; Rodriguez, V.; Pozzo, J.-L.; Ducasse, L.; Plaquet, A.; Champagne, B. Design and Characterization of Molecular Nonlinear Optical Switches. *Acc. Chem. Res.* **2013**, *46*, 2656−2665.
(15) Sliwa, M.; Létard, S.; Malfant, I.; Nierlich, M.; Lacroix, P. G.; Asahi, T.; Masuhara, H.; Yu, P.; Nakatani, K. Design, Synthesis, Structural and Nonlinear Optical Properties of Photochromic Crystals: Toward Reversible Molecular Switches. *Chem. Mater.* **2005**, *17*, 4727−4735.
(16) Boubekeur-Lecaque, L.; Coe, B. J.; Harris, J. A.; Helliwell, M.; Asselberghs, I.; Clays, K.; Foerier, S.; Verbiest, T. Incorporation of Amphiphilic Ruthenium(II) Ammine Complexes into Langmuir-Blodgett Thin Films with Switchable Quadratic Nonlinear Optical Behavior. *Inorg. Chem.* **2011**, *50*, 12886−12899.
(17) Green, K. A.; Cifuentes, M. P.; Samoc, M.; Humphrey, M. G. Metal Alkynyl Complexes as Switchable NLO Systems. *Coord. Chem. Rev.* **2011**, *255*, 2530−2541.
(18) Ségerie, A.; Castet, F.; Kanoun, M. B.; Plaquet, A.; Liégeois, V.; Champagne, B. NLO Switching Behavior in the Solid State: a Theoretical Investigation on Anils. *Chem. Mater.* **2011**, *23*, 3993−4001.
(19) Serra-Crespo, P.; van der Veen, M. A.; Gobechiya, E.; Houthoofd, K.; Filinchuk, Y.; Kirschhock, C. E. A.; Martens, J. A.; Sels, B. F.; De Vos, D. E.; Kapteijn, F.; Gascon, J. NH_2-MIL-53 (Al): a High- Contrast Reversible Solid-State Nonlinear Optical Switch. *J. Am. Chem. Soc.* **2012**, *134*, 8314−8317.
(20) De, S.; Ray, M.; Pati, A. Y.; Das, P. K. Base Triggered Enhancement of First Hyperpolarizability of a Keto-Enol Tautomer. *J. Phys. Chem. B* **2013**, *117*, 15086−15092.
(21) Li, P.-X.; Wang, M.-S.; Zhang, M.-J.; Lin, C.-S.; Cai, L.-Z.; Guo, S.-P.; Guo, G.-C. Electron-Transfer Photochromism to Switch Bulk Second-Order Nonlinear Optical Properties with High Contrast. *Angew. Chem., Int. Ed.* **2014**, *53*, 11529−11531.
(22) Matczyszyn, K.; Olesiak-Banska, J.; Olesiak-Banska, J.; Nakatani, K.; Yu, P.; Murugan, N. A.; Zaleśny, R.; Roztoczyńska, A.; Bednarska, J.; Bartkowiak, W.; Kongsted, J.; Ågren, H.; Samoć, M. One- and Two-Photon Absorption of a Spiropyran-Merocyanine System: Experimental and Theoretical Studies. *J. Phys. Chem. B* **2015**, *119*, 1515−1522.
(23) van Bezouw, S.; Campo, J.; Lee, S.-H.; Kwon, O.-P.; Wenseleers, W. Organic Compounds with Large and High-Contrast pH-Switchable Nonlinear Optical Response. *J. Phys. Chem. C* **2015**, *119*, 21658−21663.
(24) Boixel, J.; Guerchais, V.; Le Bozec, H.; Chantzis, A.; Jacquemin, D.; Colombo, A.; Dragonetti, C.; Marinotto, D.; Roberto, D. Sequential Double Second-Order Nonlinear Optical Switch by an Acido-Triggered Photochromic Cyclometallated Platinum(ii) Complex. *ChemComm* **2015**, *51*, 7805−7808.
(25) Schulze, M.; Utecht, M.; Hebert, A.; Rück-Braun, K.; Saalfrank, P.; Tegeder, P. Reversible Photoswitching of the Interfacial Nonlinear Optical Response. *J. Phys. Chem. Lett.* **2015**, *6*, 505−509.
(26) Tonnelé, C.; Champagne, B.; Muccioli, L.; Castet, F. Second-Order Nonlinear Optical Properties of Stenhouse Photoswitches: Insights from Density Functional Theory. *Phys. Chem. Chem. Phys.* **2018**, *20*, 27658−27667.
(27) Tonnelé, C.; Champagne, B.; Muccioli, L.; Castet, F. Nonlinear Optical Contrast in Azobenzene-Based Self-Assembled Monolayers. *Chem. Mater.* **2019**, *31*, 6759−6769.
(28) Avramopoulos, A.; Zaleśny, R.; Reis, H.; Papadopoulos, M. G. A Computational Strategy for the Design of Photochromic Derivatives Based on Diarylethene and Nickel Dithiolene with Large Contrast in Nonlinear Optical Properties. *J. Phys. Chem. C* **2020**, *124*, 4221−4241.
(29) Kandambeth, S.; Mallick, A.; Lukose, B.; Mane, M. V.; Heine, T.; Banerjee, R. Construction of Crystalline 2D Covalent Organic Frameworks with Remarkable Chemical (Acid/Base) Stability via a Combined Reversible and Irreversible Route. *J. Am. Chem. Soc.* **2012**, *134*, 19524−19527.
(30) DeBlase, C. R.; Silberstein, K. E.; Truong, T.-T.; Abruña, H. D.; Dichtel, W. R. β-Ketoenamine-Linked Covalent Organic Frameworks Capable of Pseudocapacitive Energy Storage. *J. Am. Chem. Soc.* **2013**, *135*, 16821−16824.
(31) Chandra, S.; Kundu, T.; Kandambeth, S.; Babarao, R.; Marathe, Y.; Kunjir, S. M.; Banerjee, R. Phosphoric Acid Loaded Azo (-N=N-) Based Covalent Organic Framework for Proton Conduction. *J. Am. Chem. Soc.* **2014**, *136*, 6570−6573.
(32) Castet, F.; Champagne, B. Switching of the Nonlinear Optical Responses of Anil Derivatives: from Dilute Solutions to the Solid State. In *Tautomerism: Concepts and Applications in Science and Technology*; Antonov, L., Ed.; Wiley-VCH: Weinheim, 2016; Chapter 8, pp 175−202.
(33) Dovesi, R.; Orlando, R.; Erba, A.; Zicovich-Wilson, C. M.; Civalleri, B.; Casassa, S.; Maschio, L.; Ferrabone, M.; De La Pierre, M.; D'Arco, P.; et al. CRYSTAL14: a Program for the Ab Initio Investigation of Crystalline Solids. *Int. J. Quantum Chem.* **2014**, *114*, 1287−1317.
(34) Dovesi, R.; Erba, A.; Orlando, R.; Zicovich-Wilson, C. M.; Civalleri, B.; Maschio, L.; Rérat, M.; Casassa, S.; Baima, J.; Salustro, S.; Kirtman, B. Quantum-Mechanical Condensed Matter Simulations with CRYSTAL. *Wiley Interdiscip. Rev.: Comput. Mol. Sci.* **2018**, *8*, No. e1360.
(35) Dovesi, R.; Pascale, F.; Civalleri, B.; Doll, K.; Harrison, N. M.; Bush, I.; D'Arco, P.; Noël, Y.; Rérat, M.; Carbonnière, P.; et al. The CRYSTAL Code, 1976−2020 and Beyond, a Long Story. *J. Chem. Phys.* **2020**, *152*, 204111.
(36) Chai, J.-D.; Head-Gordon, M. Systematic Optimization of Long-Range Corrected Hybrid Density Functionals. *J. Chem. Phys.* **2008**, *128*, 084106.
(37) Pritchard, B. P.; Altarawy, D.; Didier, B.; Gibson, T. D.; Windus, T. L. A New Basis Set Exchange: An Open, Up-to-date Resource for the Molecular Sciences Community. *J. Chem. Inf. Model.* **2019**, *59*, 4814−4820.
(38) Quertinmont, J.; Carletta, A.; Tumanov, N. A.; Leyssens, T.; Wouters, J.; Champagne, B. Assessing Density Functional Theory Approaches for Predicting the Structure and Relative Energy of Salicylideneaniline Molecular Switches in the Solid State. *J. Phys. Chem. C* **2017**, *121*, 6898−6908.
(39) Quertinmont, J.; Leyssens, T.; Wouters, J.; Champagne, B. Effects of Empirical Dispersion Energy on the Geometrical Parameters and Relative Energy of a Salicylideneaniline Molecular Switch in the Solid State. *Crystals* **2018**, *8*, 125.
(40) Ferrero, M.; Rérat, M.; Kirtman, B.; Dovesi, R. Calculation of First and Second Static Hyperpolarizabilities of One- to Three-Dimensional Periodic Compounds. Implementation in the CRYSTAL Code. *J. Chem. Phys.* **2008**, *129*, 244110.
(41) Lacivita, V.; Rérat, M.; Kirtman, B.; Ferrero, M.; Orlando, R.; Dovesi, R. Calculation of the dielectric constant ϵ and first nonlinear susceptibility $\chi(2)$ of crystalline potassium dihydrogen phosphate by the coupled perturbed Hartree-Fock and coupled perturbed Kohn-

https://dx.doi.org/10.1021/acs.jpcc.0c07672
J. Phys. Chem. C 2020, 124, 24451−24459

Sham schemes as implemented in theCRYSTALcode. *J. Chem. Phys.* **2009**, *131*, 204509.
(42) Orlando, R.; Lacivita, V.; Bast, R.; Ruud, K. Calculation of the First Static Hyperpolarizability Tensor of Three-Dimensional Periodic Compounds with a Local Basis Set: A Comparison of LDA, PBE, PBE0, B3LYP, and HF Results. *J. Chem. Phys.* **2010**, *132*, 244106.
(43) Maschio, L.; Rérat, M.; Kirtman, B.; Dovesi, R. Calculation of the dynamic first electronic hyperpolarizability$\beta(-\omega\sigma;\omega1,\omega2)$ of periodic systems. Theory, validation, and application to multi-layer MoS2. *J. Chem. Phys.* **2015**, *143*, 244102.
(44) Rérat, M.; Maschio, L.; Kirtman, B.; Civalleri, B.; Dovesi, R. Computation of Second Harmonic Generation for Crystalline Urea and KDP. An Ab Initio Approach through the Coupled Perturbed Hartree−Fock/Kohn−Sham Scheme. *J. Chem. Theory Comput.* **2016**, *12*, 107−113.
(45) Zhang, Y.; Champagne, B. Theoretical Insight Into the Second-Order NLO Response of the Bis {4-[2-(4-Pyridyl) Ethenyl] Benzoato}-Zinc(II) Metal-Organic Framework. *J. Phys. Chem. C* **2012**, *116*, 21973−21981.
(46) Seidler, T.; Stadnicka, K.; Champagne, B. Evaluation of the Linear and Second-Order NLO Properties of Molecular Crystals Within the Local Field Theory: Electron Correlation Effects, Choice of XC Functional, ZPVA Contributions, and Impact of the Geometry in the Case of 2-Methyl-4-Nitroaniline. *J. Chem. Theory Comput.* **2014**, *10*, 2114−2124.
(47) Seidler, T.; Champagne, B. Second-Order Nonlinear Optical Susceptibilities of Metal−Organic Frameworks Using a Combined Local Field Theory/Charge Embedding Electrostatic Scheme. *J. Phys. Chem. C* **2016**, *120*, 6741−6749.
(48) Fang, Z.; Lin, J.; Liu, R.; Liu, P.; Li, Y.; Huang, X.; Ding, K.; Ning, L.; Zhang, Y. Computational Design of Inorganic Nonlinear Optical Crystals Based on a Genetic Algorithm. *CrystEngComm* **2014**, *16*, 10569−10580.
(49) Ni, B.; Sun, W.; Kang, J.; Zhang, Y. Understanding the Linear and Second-Order Nonlinear Optical Properties of UiO-66-Derived Metal−Organic Frameworks: A Comprehensive DFT Study. *J. Phys. Chem. C* **2020**, *124*, 11595−11608.
(50) Castet, F.; Bogdan, E.; Plaquet, A.; Ducasse, L.; Champagne, B.; Rodriguez, V. Reference Molecules for Nonlinear Optics: A Joint Experimental and Theoretical Investigation. *J. Chem. Phys.* **2012**, *136*, 024506.
(51) Brasselet, S.; Zyss, J. Multipolar Molecules and Multipolar Fields: Probing and Controlling the Tensorial Nature of Nonlinear Molecular Media. *J. Opt. Soc. Am. B* **1998**, *15*, 257−288.
(52) Rodriguez, V.; Grondin, J.; Adamietz, F.; Danten, Y. Local Structure in Ionic Liquids Investigated by Hyper-Rayleigh Scattering. *J. Phys. Chem. B* **2010**, *114*, 15057−15065.
(53) Tuer, A.; Krouglov, S.; Cisek, R.; Tokarz, D.; Barzda, V. Three-Dimensional Visualization of the First Hyperpolarizability Tensor. *J. Comput. Chem.* **2011**, *32*, 1128−1134.
(54) Liégeois, V. *DrawMol*; UNamur, www.unamur.be/drawmol.
(55) Zutterman, F.; Louant, O.; Mercier, G.; Leyssens, T.; Champagne, B. Predicting Keto−Enol Equilibrium from Combining UV/Visible Absorption Spectroscopy with Quantum Chemical Calculations of Vibronic Structures for Many Excited States. A Case Study on Salicylideneanilines. *J. Phys. Chem. A* **2018**, *122*, 5370−5374.
(56) Barboza, C. A.; Sobolewski, A. L. An *Ab Initio* Study on the Photophysics of Tris(Salicylideneaniline). *Phys. Chem. Chem. Phys.* **2018**, *20*, 25164−25168.
(57) Halbout, J.-M.; Blit, S.; Donaldson, W.; Chung Tang, C. L. Efficient Phase-Matched Second-Harmonic Generation and Sum-Frequency Mixing in Urea. *IEEE J. Quantum Electron.* **1979**, *15*, 1176−1180.
(58) Morita, R.; Kondo, T.; Kaneda, Y.; Sugihashi, A.; Ogasawara, N.; Umegaki, S.; Ito, R. Multiple-Reflection Effects in Optical Second-Harmonic Generation. *Jpn. J. Appl. Phys.* **1988**, *27*, L1134−L1136.
(59) Bogdan, E.; Plaquet, A.; Antonov, L.; Rodriguez, V.; Ducasse, L.; Champagne, B.; Castet, F. Solvent Effects on the Second-Order Nonlinear Optical Responses in the Keto-Enol Equilibrium of a 2-Hydroxy-1-naphthaldehyde Derivative. *J. Phys. Chem. C* **2010**, *114*, 12760−12768.
(60) Guillaume, M.; Champagne, B.; Markova, N.; Enchev, V.; Castet, F. Ab Initio Investigation on the Second-Order Nonlinear Optical Responses in Keto-Enol Equilibrium of Salicylideneanilines. *J. Phys. Chem. A* **2007**, *111*, 9914−9923.
(61) Champagne, B.; Plaquet, A.; Pozzo, J.-L.; Rodriguez, V.; Castet, F. Nonlinear Optical Molecular Switches as Selective Cation Sensors. *J. Am. Chem. Soc.* **2012**, *134*, 8101−8103.

https://dx.doi.org/10.1021/acs.jpcc.0c07672
J. Phys. Chem. C 2020, 124, 24451−24459